Light triggers expression of philanthotoxin-insensitive Ca2+-permeable AMPA receptors in the developing rat retina

Ingrid K. Osswald, Alba Galan and Derek Bowie

J. Physiol. 2007;582;95-111; originally published online Apr 12, 2007;

DOI: 10.1113/jphysiol.2007.127894

Light triggers expression of philanthotoxin-insensitive Ca^{2+}-permeable AMPA receptors in the developing rat retina

Ingrid K. Osswald*, Alba Galan* and Derek Bowie

Department of Pharmacology & Therapeutics, McGill University, Montreal, Quebec, Canada

Ca^{2+}-permeable AMPA receptors (AMPARs) are expressed throughout the adult CNS but yet their role in development is poorly understood. In the developing retina, most investigations have focused on Ca^{2+} influx through NMDARs in promoting synapse maturation and not on AMPARs. However, NMDARs are absent from many retinal cells suggesting that other Ca^{2+}-permeable glutamate receptors may be important to consider. Here we show that inhibitory horizontal and AII amacrine cells lack NMDARs but express Ca^{2+}-permeable AMPARs. Before eye-opening, AMPARs were fully blocked by philanthotoxin (PhTX), a selective antagonist of Ca^{2+}-permeable AMPARs. After eye-opening, however, a subpopulation of Ca^{2+}-permeable AMPARs were unexpectedly PhTX resistant. Furthermore, Joro spider toxin (JSTX) and IEM-1460 also failed to antagonize, demonstrating that this novel pharmacology is shared by several AMPAR channel blockers. Interestingly, PhTX-insensitive AMPARs failed to express in retinae from dark-reared animals demonstrating that light entering the eye triggers their expression. Eye-opening coincides with the consolidation of inhibitory cell connections suggesting that the developmental switch to a Ca^{2+}-permeable AMPAR with novel pharmacology may be critical to synapse maturation in the mammalian retina.

(Received 8 January 2007; accepted after revision 10 April 2007; first published online 12 April 2007)
Corresponding author D. Bowie: Department of Pharmacology & Therapeutics, McIntyre Medical Sciences Building, Room 1317, McGill University, 3655 Promenade Sir William Osler, Montreal, Québec, Canada H3A 1Y6.
Email: derek.bowie@mcgill.ca

AMPA ionotropic glutamate receptors (iGluRs) are prominent excitatory neurotransmitter receptors expressed in the CNS. They assemble as tetramers from four possible subunits (i.e. GluR1–4) that impart distinct functional properties (Dingledine *et al.* 1999). The GluR2 subunit is critical since it regulates important characteristics such as Ca^{2+} permeability (Burnashev, 1996), external and internal polyamine block (Bowie *et al.* 1999), the pore's unitary conductance (Dingledine *et al.* 1999) as well as subunit assembly and stoichiometry (Greger *et al.* 2003). GluR2 homomers are Ca^{2+} impermeable, insensitive to polyamine block and exhibit a small unitary conductance (Bowie *et al.* 1999; Dingledine *et al.* 1999). In contrast, GluR2-lacking AMPARs are Ca^{2+} permeable, blocked by polyamines and exhibit large single-channel currents (Bowie *et al.* 1999; Dingledine *et al.* 1999). Although most synaptic AMPARs are GluR2-containing heteromers (Dingledine *et al.* 1999), discrimination between Ca^{2+}-permeable and -impermeable isoforms has been difficult to achieve using ion-permeability measurements or imaging studies. As an alternative, polyamines, such as PhTX, have been used as pharmacological markers of Ca^{2+}-permeable AMPARs (Toth & McBain, 1998; Laezza *et al.* 1999; Liu & Cull-Candy, 2000; Thiagarajan *et al.* 2005; Plant *et al.* 2006; Ge *et al.* 2006). This approach is based on the observation that recombinant AMPAR heteromers are rendered Ca^{2+} impermeable with fewer GluR2 subunits than required to eliminate polyamine block (Washburn *et al.* 1997; Cull-Candy *et al.* 2006). Consequently, AMPARs sensitive to external polyamine block are considered, from a conservative standpoint, to be Ca^{2+} permeable whereas the absence of block identifies Ca^{2+}-impermeable isoforms.

Although Ca^{2+}-permeable AMPARs are expressed sparingly, they serve important roles in CNS physiology and pathology. Ca^{2+} influx following AMPAR stimulation is associated with long-term plasticity at neuronal (Laezza *et al.* 1999; Liu & Cull-Candy, 2000) as well as neuron–glial (Ge *et al.* 2006) synapses. In contrast, relief from polyamine block (Bowie *et al.* 1998) provides synaptic AMPARs with

*I. K. Osswald and A. Galan contributed equally to this work.

DOI: 10.1113/jphysiol.2007.127894

a novel form of short-term plasticity (Rozov & Burnashev, 1999). In disease states, Ca^{2+}-permeable AMPARs have been implicated in ischaemia (Liu *et al.* 2004), epilepsy (Krestel *et al.* 2004) and the growth of glioblastomas (Ishiuchi *et al.* 2002). Despite this understanding of Ca^{2+}-permeable AMPARs, little is known of their role in development. In the retina, for example, although glutamatergic transmission is known to drive propagating Ca^{2+} waves during development (Wong *et al.* 2000), all investigations so far have focused on the role of NMDARs (Wong & Wong, 2000; van Zundert *et al.* 2004).

Here, we have used a multidisciplinary approach to examine Ca^{2+}-permeable AMPARs during postnatal development of the mammalian retina. We show that Ca^{2+}-permeable AMPARs are primarily expressed in the rat retina by two inhibitory cell types, horizontal and AII amacrine cells. Prior to eye-opening, Ca^{2+}-permeable AMPARs are fully blocked by PhTX as reported elsewhere in the CNS. Unexpectedly however, after eye-opening, Ca^{2+}-permeable AMPARs exhibit insensitivity to PhTX. This developmental switch occurs at a time point when neuronal connections are being established with presynaptic bipolar cells suggesting that synapses of distinct Ca^{2+}-permeable AMPARs may fulfil important roles in synapse maturation.

Methods

Dissection of the retina and slice preparation

All experiments were performed on neonatal and adult Sprague–Dawley rats (male or female). Light-adapted animals were maintained on a 12 h light–dark cycle in accordance with the guidelines established by the Canadian Council on Animal Care. For light-deprived animals, pregnant mothers were housed in a separate room devoid of light and therefore pups were dark-reared from birth. In such cases, animals and the preparation of tissue was performed in a dim infrared light source to ensure strict conditions of light deprivation. All rats were decapitated under deep isoflurane anaesthesia, eyes were enucleated and hemisected in a cutting solution containing 233 mM sucrose, 7 mM D(+) glucose, 7 mM $MgCl_2$, 3.75 mM sodium pyruvate, 2.5 mM KCl, 1.25 mM NaH_2PO_4, 1 mM ascorbic acid, 0.5 mM $CaCl_2$, pH 7.4. The retina was then carefully detached from the pigment epithelium and sclera using a pair of fine dissecting forceps (No. 4, Dumostar).

For cobalt staining, the retina was cut into four pieces and oxygenated with 95% O_2–5% CO_2 at room temperature (22°C) for 30 min. For electrophysiology, the retina was chilled to 4°C with ice slush prepared from oxygenated cutting solution. The retina was then transferred in cutting solution to the upper surface of a small cube of 4% agar. The retina was drained of excess cutting solution using absorbent tissue and promptly annealed to the agar cube using a drop of 2% low melting point agar prepared at 42°C in 119 mM NaCl, 2.5 mM KCl, 10 mM glucose, 26 mM Hepes, 1.25 mM Na_2HPO_4, 2 mM sodium pyruvate, 0.5 mM ascorbic acid, 2.5 mM $CaCl_2$, 1.5 mM $MgCl_2$, pH 7.4. The ensemble was then fixed to the platform of a vibratome (Leica, VT1000S) using cyanoacrylate adhesive and rapidly immersed into ice-cold oxygenated cutting solution. Slices of 200 μm were obtained, transferred to ACSF (125 mM NaCl, 2.5 mM KCl, 25 mM $NaHCO_3$, 2.5 mM $CaCl_2$, 1 mM $MgCl_2$, 10 mM glucose, 2 mM sodium pyruvate, 0.5 mM ascorbic acid, pH 7.4 using 5 N NaOH) and oxygenated at room temperature.

Cobalt staining technique

Ca^{2+}-permeable AMPARs were identified using a modified protocol of the cobalt (Co^{2+}) staining technique (Pruss *et al.* 1991). Experiments were performed in either normal light or infrared condition. In each case, dissected retina were first incubated for 30 min in oxygenated assay buffer (5 mM KCl, 2 mM $MgCl_2$, 12 mM glucose, 20 mM bicarbonate, 139 mM sucrose, 57.5 mM NaCl and 0.75 mM $CaCl_2$) which, when required, provided a sufficient period to allow receptor antagonists to equilibrate with the tissue. The retina pieces were then stimulated each for 15 min in oxygenated assay buffer containing 5 mM $CoCl_2$ with saturating agonist concentration (L-glutamic acid (10 mM L-Glu), *N*-methyl-D-aspartate (50 μM NMDA) or (L)-(+)-2-amino-4-phosphonobutyric acid (40 μM AP4)) in the presence or absence of GluR antagonists (6-cyano-7-nitroquinoxaline-2,3-dione (20 μM CNQX) (DL)-2-amino-5-phosphonovaleric acid (40 μM APV), 4-(8-methyl-9H-1,3-dioxolo[4,5-h][2,3]benzodiazepine-5-yl)-benzenamine hydrochloride (40 μM GYKI 52466) (*RS*)-α-cyclopropyl-4-phosphonophenylglycine (40 μM CPPG)). Channel blockers, PhTX 343 tris(trifluoroacetate) salt and IEM-1460, were purchased from Sigma, and Joro spider toxin-3 (JSTX) was a gift from Dr Heather Durham (Montreal Neurological Institute, McGill University). All other drugs were purchased from Tocris (Missouri, USA), stored frozen in stock solutions at −20°C and were then diluted into ACSF or assay buffer as required. Retina pieces were then rinsed in assay buffer and incubated in 2 mM EDTA for 5 min to remove excess Co^{2+}. After an additional rinse, Co^{2+} was precipitated with 0.24% ammonium sulphide in assay buffer and the retina fixed for 4 h in 0.8% glutaraldehyde in phosphate buffer. Each retina piece was cryoprotected overnight at 4°C in phosphate buffer saline (PBS) containing 30% sucrose. The retina was then embedded in OCT (Tissue Tek, CA, USA) and snap-frozen at −50°C with 2-methylbutane. Sections of 20 μm were cut on a cryostat (2700 Frigocut, Riechert-Jung) and rinsed

with distilled water. Silver enhancement of the cobalt sulphide precipitate was performed using the intenSE kit (Amersham, USA). The enhancement step is both time- and temperature-sensitive. To obtain the optimal reaction time (~30–40 min), we routinely constructed a calibration curve of Co^{2+} staining at different time points at room temperature. After silver enhancement, each retinal section was rinsed and mounted in 10% glycerol in PBS. Photomicrograph images were captured with a Zeiss Axioplan 2 Imaging microscope equipped with a high resolution colour digital camera and connected to a computer with Zeiss Axiovision 4.1 Software (Zeiss, Canada). Photomicrographs were obtained with a 40× objective and stored in the Zeiss Axiovision format. To avoid variation in staining intensity, the exposure settings of the digital camera for all samples were kept constant. Moreover, staining between control and treated conditions shown in all figures of this study were compared from retina taken from the same animal and that was processed for Co^{2+} staining in parallel. To ensure reproducibility, all Co^{2+} staining experiments shown in this study were repeated on several retinae pieces from at least three different animals.

Image analysis and quantification

Images from bright-field microscopy were obtained in black and white format and imported into an MCID Elite Image Analysis system (Imaging Research Inc., St Catharines, Ontario, Canada). In each case, measurements of the relative optical density were performed by the system within the limits of a rectangle of 90 μm × 8.1 μm which was applied to the outer or inner plexiform layers (OPL or IPL) of the retina that included either horizontal cells or sublamina a and b, respectively. A total number of eight images were obtained per retina slice which was repeated for eight adult rats. The data between different treatments were compared using a paired *t* test and expressed as the mean ± S.E.M.

Immunohistochemistry

Retina pieces prepared for Co^{2+} staining were used for immunofluorescence. In this case, however, each retina piece was fixed using 4% paraformaldehyde in 0.2 M phosphate buffer at pH 7.4 for 2 h and cryoprotected in 30% sucrose buffer overnight at 4°C. Retinae were embedded in OCT Tissue Tek and frozen as previously described. Sections of 20 μm were then cut on a cryostat and processed for confocal microscopy as on-slide sections. Briefly, slides were rinsed three times for 5 min in 0.1 M PBS–0.3% Triton X-100 (PBS-T) and blocked in 10% normal goat serum in PBS-T. Sections were incubated overnight with a rabbit anti-calbindin-D 28K antibody (1 : 2000, Sigma) a specific marker for horizontal cells (Oguni *et al.* 1998). Slides were subsequently washed as before in PBS-T and incubated with a goat anti-rabbit IgG Alexa 488 (1 : 800, Molecular Probes, USA) secondary antibody. After washing in PBS, slides were mounted using an anti-fading medium (Vectashield, Vector Laboratories) and observed on a Zeiss 510 LSM confocal microscope.

Electrophysiology recordings

Acutely isolated retinal slices were visualized using an infrared (IR) video camera (Dage-MTI, Michigan City, IN, USA) attached to an upright microscope (Olympus, Japan) that was equipped with 60× differential interference contrast (DIC) objective. AII amacrine cells were visually identified by their thick dendritic processes and triangular-shaped cell bodies that were positioned at the junction of the inner nuclear (INL) and plexiform layers (IPL) (Fig. 2*A*). In contrast, cell bodies of horizontal cells were oval-shaped, much larger in size and were positioned horizontally in the proximal region of the INL (Fig. 2*B*). The identity of each cell type was confirmed *post hoc* using Lucifer Yellow to provide complete visualization of dendritic morphology. All whole-cell recordings were performed on light-adapted retina using borosilicate glass pipettes (7–10 MΩ) and a MultiClamp 700A amplifier (Axon Instruments, Union City, CA, USA) in voltage-clamp mode. Membrane currents were digitized at 5 kHz using the Digidata 1322A (Axon Instruments) and filtered at 2.5 kHz using a low-pass Bessel filter (Frequency Devices, MA, USA). Cells with series resistances < 25 MΩ that were compensated up to 80% were used for analysis. In all cases, recordings were monitored to ensure stability in series resistance and the event amplitude. AII amacrine cells and horizontal cells had cell capacitances of 13.7 ± 5.2 pF ($n = 30$) and 42.4 ± 15.9 pF ($n = 8$), respectively. All recordings were performed at room temperature (22°C). In experiments performed on dark- reared animals, the entire electrophysiological experiment was performed in dim infrared conditions.

Oxygenated ACSF used to bathe retinal slices routinely contained bicuculline (10 μM) and strychnine (1 μM) to block GABAergic and glycinergic synaptic activity. Although presynaptic $GABA_C$ receptors expressed by rod bipolar cells are not blocked by bicuculline (Lukasiewicz *et al.* 2004), their activation regulates the frequency of glutamatergic activity onto AII cells which was not examined in this study. In experiments where miniature synaptic events were recorded, tetrodotoxin (TTX, 0.5 μM) was also added to the ACSF to eliminate spontaneous activity. The internal solution contained 125 mM $CsCH_3SO_3$, 5 mM Hepes, 4 mM Na_2ATP, 5 mM Cs_4BAPTA, 1 mM $CaCl_2$, 2 mM QX-314 bromide to block

sodium channels and 0.5% biocytin HCl with 0.5 mg ml^{-1} Lucifer Yellow to visualize cell morphology. pH was adjusted to 7.4 with 5 N CsOH. Local agonist/antagonist applications were performed using a homemade flowpipe from theta tubing that had been pulled to a final tip diameter of 300–400 μm. The tip of the theta tubing was routinely placed within 1 mm of the cell chosen for study.

Data analysis

Data acquisition and analysis was performed using pCLAMP9 (Molecular Devices) software and illustrated using Origin 7 (Microcal, Northampton, MA, USA). Extended structures of channel blockers (Fig. 6*A*) were drawn using ChemDraw 8 (CambridgeSoft, Cambridge, MA, USA). Miniature and spontaneous synaptic activity was analysed using WinEDR (Windows Electrophysiology Disk Recorder) that was kindly provided by Dr John Dempster (Strathclyde University, UK). Synaptic events were primarily detected by an amplitude threshold algorithm set to identify events that were four times the standard deviation of baseline noise. This was followed by visual confirmation to eliminate false positives due to variable baseline noise levels or multiphasic events. The threshold method did not affect the outcome of analysis described in this study since similar results were achieved using a template-based algorithm for event detection (Clements & Bekkers, 1997). Data were rejected for analysis if it showed signs of time-dependent decline in amplitude or of the kinetic parameters. Amplitude distributions were fitted by the sum of two to three Gaussian functions of the singular form:

$$y = (\text{Area}/(\text{Variance} \times \text{v}(\pi/2))) \times \exp(-2((x - \text{Peak})/\text{Variance})^2)$$

where y refers to the number of observed events and x to the peak amplitude which has units of picoamps. For Gaussian fits of pooled data (e.g. Figs 7 and 10), biasing was avoided by selecting a similar number of events from each cell. The number of Gaussian functions required to fit amplitude distributions is model independent and therefore is not used in this study to indicate distinct populations of AMPAR synapses. Likewise, the distribution of decay kinetics was fitted by the sum of two to three exponential functions that were used in this study in a model-independent manner.

Biocytin labelling

After completion of each electrophysiological experiment, retina slices were fixed in 4% paraformaldehyde for 30 min at room temperature and stored at 4°C until processed for biocytin staining. Retina slices were then washed in sterile PBS and incubated for 10 min in PBS containing 10% methanol and 1% H_2O_2. They were subsequently washed and transferred for 1 h to 2% Triton dissolved in PBS. A standard reaction of diaminobenzidine was then performed using the ABC kit from Vectastain (Burlingame, CA, USA). After washes, slices were processed for 30 min using 3,3′-diaminobenzidine (DAB) prepared with 1% $CoCl_2$ and 1% $NiCl_2$, rinsed and mounted in 10% glycerol in PBS.

Results

Ca^{2+}-permeable AMPARs are expressed primarily by inhibitory cells

The distribution of Ca^{2+}-permeable AMPARs was initially examined in the adult rat retina using Co^{2+} staining. The advantage of this technique is that divalent-permeable AMPARs will transport other divalent ions, such as Co^{2+}, in addition to Ca^{2+}. The transported Co^{2+} can then be revealed as a dark brown precipitate identifying the cell expressing Ca^{2+}-permeable AMPARs. All Co^{2+} staining experiments shown in this study were repeated on several retinae pieces from animals taken from at least three different rat litters. Figure 1 (left panel) shows a photomicrograph of a transverse section of the adult retina (i.e. 3 months old) stained with Co^{2+} following stimulation with 10 mM L-glutamate (L-Glu). Two populations of cell bodies were primarily stained with Co^{2+} with their processes visible either as lateral or vertical extensions labelled in the outer or inner plexiform layers (OPL or IPL), respectively (Fig. 1, left panel). Cells stained at the OPL–INL interface are consistent with inhibitory horizontal cells based on their morphology and immunopositive staining with the selective marker, calbindin (Oguni *et al.* 1998) (Fig. 1, upper middle panel). Cells stained at the INL–IPL interface are consistent with AII (A2) amacrine cells, another inhibitory cell in the mammalian retina (Famiglietti & Kolb, 1975). In agreement with this, injection of biocytin into visually identified AII cells in acutely isolated retinal slices revealed that the position of the cell body and that of the proximal dendrites closely matched that of Co^{2+} stained cells (Fig. 1, lower middle panels).

Co^{2+} staining with L-Glu is due to Ca^{2+}-permeable AMPARs and not other GluRs subtypes for several reasons. First, Co^{2+} staining was blocked by GYKI 52466 (40 μM), a selective AMPA-receptor antagonist (Dingledine *et al.* 1999) (Fig. 1) and not APV (20 μM) or CPPG (40 μM) which block NMDARs or metabotropic GluRs (mGluRs), respectively (Fig. 1, right). Second, selective agonists NMDA (50 μM) or AP4 (40 μM) failed to stain the retina (Fig. 1, right) confirming that Co^{2+} staining by L-Glu does not involve NMDARs or mGluRs. Third, Co^{2+} does not enter cells via voltage-gated Ca^{2+} channels since depolarization with 50 mM KCl failed to elicit staining

(data not shown) consistent with the known blocking effect of Co^{2+} on Ca^{2+} channels. As described below, complementary electrophysiological experiments further demonstrate that, unlike other retinal cells, the primary route of Ca^{2+} entry into horizontal and AII amacrine cells during glutamatergic transmission is via AMPA and not NMDA iGluRs.

Inhibitory cells express synaptic AMPARs but not NMDARs

The contribution of AMPA and NMDARs to glutamatergic transmission was assessed by the ability of subtype-selective iGluR antagonists to block excitatory postsynaptic currents (EPSCs) (Fig. 2). To do this, AII and horizontal cells were first visually identified in retinal slices by morphology (Fig. 2*A* and *B*) and later confirmed by intracellular filling with Lucifer yellow. As expected from Co^{2+} experiments, individual AII and horizontal cells responded robustly to local application of non-NMDAR agonists such as kainate (50 μM KA, Fig. 2*C*) and L-Glu (10 mM, not shown). Moreover, EPSCs and responses to exogenous agonists on AII cells were equally sensitive to CNQX (Fig. 2*C*, $n = 11$) further validating the complementary nature of Co^{2+} labelling and electrophysiological data. In contrast, individual EPSCs were poorly resolved in horizontal cells due to the membrane noise ($n = 8$) and, in some cases, an appreciable holding current between -20 to -100 pA was present ($n = 3$, Fig. 2*D*). In each cell type, however, synaptic activity was insensitive to the NMDAR antagonist APV (40 μM, Fig. 2*E* and *F*) but completely abolished by GYKI 52466 (40 μM, $n = 4$ for each cell type) (Fig. 2*E* and *F*) demonstrating that horizontal and AII amacrine cell synapses express AMPARs with little or no contribution from NMDARs. In support of this, Kalloniatis *et al.* (2004) used functional labelling with the organic cation agmatine to conclude that horizontal cells of the rabbit retina also do not express NMDARs. Interestingly, Hartveit & Veruki (1997) have described responses elicited by AII cells following bath application of NMDA suggesting that, although this inhibitory cell population expresses NMDARs, they are excluded from the postsynaptic density.

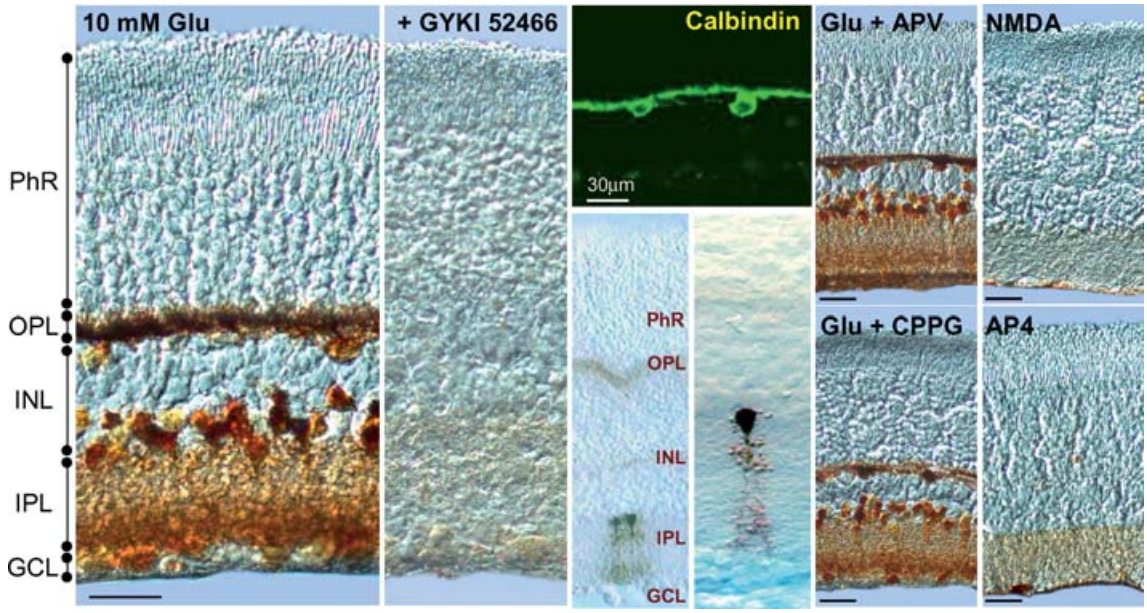

Figure 1. Ca^{2+}-permeable AMPARs are expressed by inhibitory cells of the mammalian retina
Left panels, photomicrograph of Co^{2+} staining routinely observed with 10 mM L-Glu in a 3-month-old adult rat retina (slide no. 290306-1L). Staining was restricted to processes of the outer and inner plexiform layers as well as cell bodies of horizontal and AII amacrine cells. Co^{2+} staining elicited by 10 mM L-Glu was abolished by pretreatment with 40 μM GYKI 52466, an AMPAR selective antagonist. Middle upper panel, photomicrograph of calbindin immunofluorescence identifying the cell bodies and processes of horizontal cells. Middle panel, lower right and left, photomicrographs of visually identified AII amacrine cells filled with biocytin to reveal the location of the cell body in the INL and extension of dendritic processes. Right panels, Co^{2+} staining elicited by 10 mM L-Glu was unaffected by pretreatment with NMDA or the mGluR antagonists, APV (40 μM) (slide no. 070406-3L) and CPPG (300 μM) (slide no. 070406-9L), respectively. NMDA and group III mGluR agonists, NMDA (50 μM) (slide no. 070406-5R) and L-AP4 (100 μM) (slide no. 070406-9L), respectively, also failed to produce appreciable staining suggesting that inhibitory cells accumulate Co^{2+} due to the activation of AMPARs. Unless otherwise stated, scale bars represent 20 μm.

Expression of Ca^{2+}-permeable AMPARs prior to eye-opening

To examine if both horizontal and AII amacrine cells express Ca^{2+}-permeable AMPARs throughout retinal development, we studied their distribution in the postnatal rat retina before (P1 to P11, Fig. 3) and after eye-opening (P14 to 6 months, Fig. 4). All retinal cell types are present in the rat retina prior to eye-opening (i.e. < P10) (Rapaport *et al.* 2004) whereas synaptic contacts undergo further refinement before and after eye-opening (i.e. P1–P21) (Mumm *et al.* 2005; Morgan *et al.* 2006). In view of this, eye-opening is an important marker of distinct developmental phases in the rodent retina. It is not that eye opening *per se* is causative but, as discussed below, that the visual experience of light entering the eye triggers important activity-dependent events. At birth, the rat retina has immature morphology with a prominent neuroblastic layer though the outer segment of the photoreceptor layer is absent (Fig. 3, top outerleft). In comparison, a few days prior to eye-opening (e.g. P11), the retina exhibits adult-like morphology with a clear separation

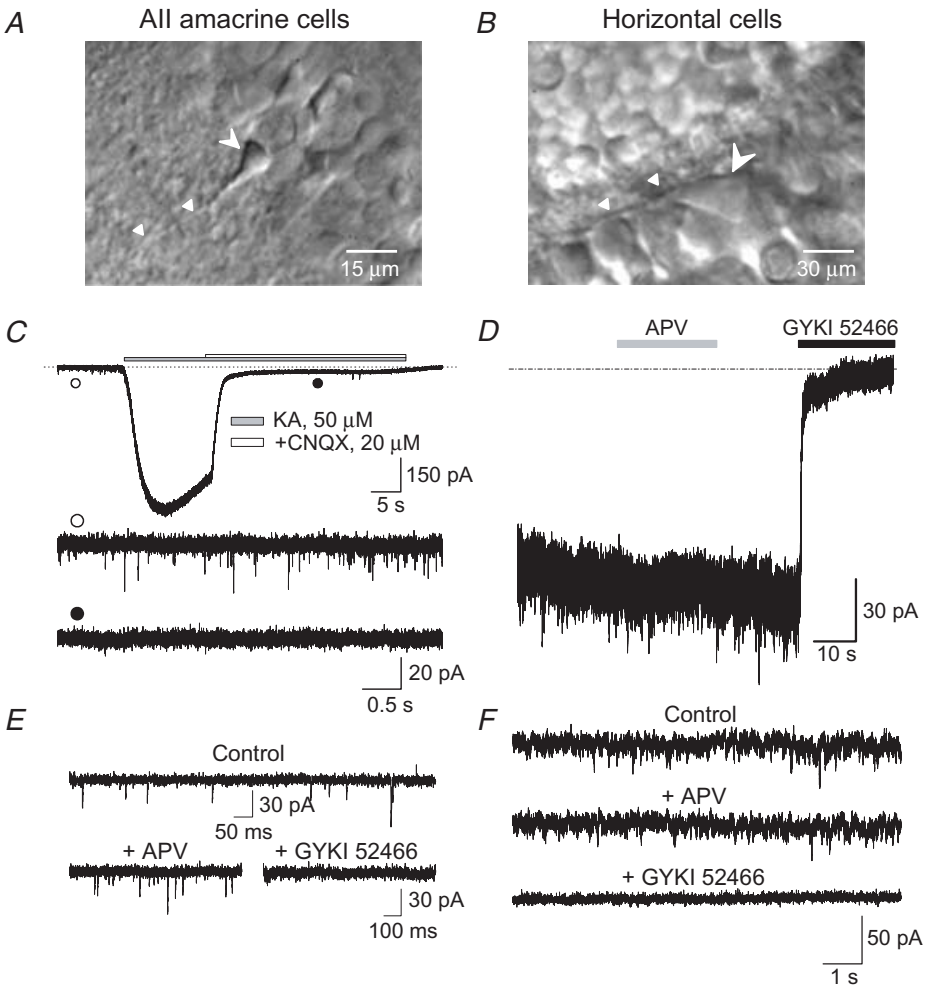

Figure 2. Horizontal and AII amacrine cells express synaptic AMPARs but not NMDARs
A, videomicrograph showing the position of the cell body close to the IPL (see arrowhead) and prominent dendrite characteristic of AII amacrine cells (see triangles) in acute retinal slice preparations. *B*, videomicrograph identifying the large triangular cell body of a typical horizontal cell (see arrowhead) and lateral dendritic processes (see triangles). *C*, whole-cell recording ($V_h = -60$ mV) from an AII cell showing spontaneous postsynaptic events (○) and inward current elicited by local application of 50 μM KA (cell no. 051208c3). Bath application of the non-NMDAR antagonist, CNQX (20 μM), blocked both spontaneous synaptic events and membrane current elicited by KA (●). *D*, whole-cell recording ($V_h = -60$ mV) from a horizontal cell showing that the spontaneous activity and holding current were insensitive to APV (40 μM), but blocked by GYKI 52466 (40 μM) (cell no. 060620c1). *E*, spontaneous events recorded from another AII amacrine cell (cell no. 060516c3, $V_h = -60$ mV) were insensitive to APV but blocked by GYKI 52466. *F*, spontaneous events recorded from the same horizontal cell as in *D* showing in more detail that synaptic activity was insensitive to APV but blocked by GYKI 52466.

of plexiform and nuclear layers (Fig. 3, top innerleft). Consistent with this maturation pattern, Co^{2+} staining from P1 to P11 retinae showed signs of cell migration as well as morphological refinement (Fig. 3). For example, although immature horizontal cells have clearly migrated to their outer position in the retina shortly after birth (e.g. P1), further dendritic refinement is apparent at stages P4 and P7 (Fig. 3, bottom left). These cells can be identified as horizontal cells since they were immunopositive to calbindin (data not shown). Cells labelled in the inner region of the retina between P1 and P7 are most likely immature amacrine cells which have more distinctive staining by P11. Interestingly, like the adult retina (Fig. 1), Co^{2+} staining of the ganglion cell layer (GCL) and INL suggests that AII cells are not the only cell type in this region of the retina labelled at P11 (Fig. 3, see below). As expected of Ca^{2+}-permeable AMPARs (Washburn *et al.* 1997; Toth & McBain, 1998), Co^{2+} staining was completely abolished from P1 to P7 by PhTX (50 μM) (Fig. 3), a polyamine channel blocker of Ca^{2+}-permeable non-NMDARs (Bowie *et al.* 1998). At P11, however, Co^{2+} staining was not fully blocked in both horizontal and amacrine cells (Fig. 3). The differential effect of PhTX cannot be explained by differences in the total number of AMPARs expressed by individual cells since the intensity of staining in all cases was comparable. Consequently, pharmacologically distinct Ca^{2+}-permeable AMPARs are apparently expressed in the developing retina.

Both external polyamine block and Ca^{2+} permeability are determined by the copy number of GluR2 subunits in mature AMPAR tetramers (Washburn *et al.* 1997; Bowie *et al.* 1999; Dingledine *et al.* 1999). Loss of polyamine block is proposed to require the inclusion of more GluR2 receptor subunits per tetramer than for the loss of divalent permeability (Washburn *et al.* 1997). Consequently, it is not possible to assemble mature AMPARs that exhibit divalent permeability whilst having little or no sensitivity to polyamine block (Washburn *et al.* 1997; Bowie *et al.* 1999). In view of this, our observation that Ca^{2+}-permeable AMPARs are insensitive to polyamine block is difficult to reconcile with current understanding of recombinant AMPARs.

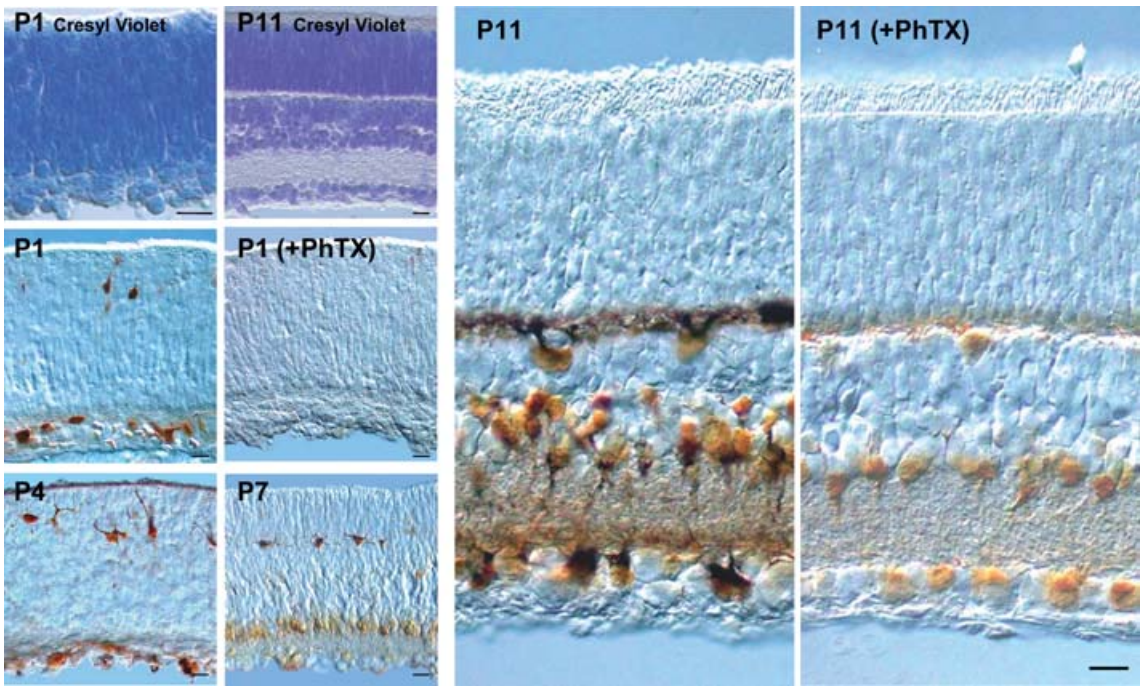

Figure 3. Expression of Ca^{2+}-permeable AMPARs before eye-opening
Top left, outer and inner panels, cresyl violet staining of retina reveals an immature retina morphology at P1 (slide no. 090405-3L) with a prominent neuroblastic layer compared with the well-defined cell layers seen at P11 (slide no. 190405-5L). Middle left, outer and inner panels, Co^{2+} staining at P1 (slide no. 090405-7L) was blocked by 50 μM PhTX revealing the presence of Ca^{2+}-permeable AMPARs at birth. Bottom left, outer and inner panels, Co^{2+} staining with 10 mM L-Glu in P4 (slide no. 120405-6L) and P7 (slide no. 150405-10L) retinae showing the migration and maturation of horizontal and amacrine cells. Middle and right panels, Co^{2+} staining elicited by L-Glu at P11 (slide no. 190405-2R) failed to be completely blocked by 50 μM PhTX suggesting that Ca^{2+}-permeable AMPARs develop insensitivity to polyamine block a few days before eye-opening. Scale bars represent 10 μm in all cases.

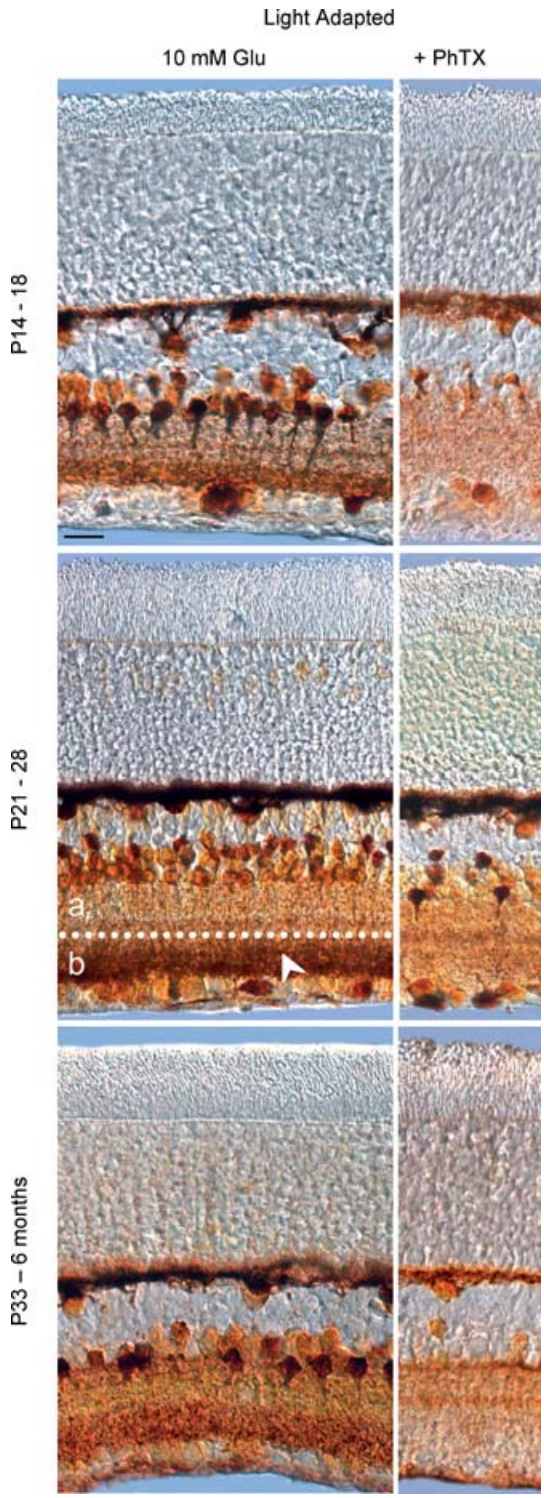

Figure 4. Inhibitory cells express PhTX-insensitive Ca^{2+}-permeable AMPARs after eye-opening
Left panels, after eye-opening horizontal and AII amacrine cells were strongly labelled by Co^{2+} at all developmental stages tested (P14–18, slide no. 220405-7R; P21–28, slide no. 250405-8R; P33–6 months: slide no. 260105-11L). Expression patterns in the INL are further refined during development with the transient expression of Ca^{2+}-permeable AMPARs in another amacrine cell population(s) that may be A17 cells. Note there is a greater intensity of staining in sublamina b of the IPL (see arrowhead). Right panels, PhTX failed to fully block Co^{2+} staining after eye-opening at all developmental stages. Horizontal cell dendrites in particular were completely insensitive to block by PhTX. For AII cells, Co^{2+} staining of cell bodies was initially PhTX insensitive (P14–18, slide no. 220405-7R; P21–28, slide no. 250405-8R, respectively). However, at later stages, the staining of cell bodies was abolished by PhTX. In contrast, staining of the IPL was resistant to PhTX block at all stages.

PhTX-insensitive Ca^{2+}-permeable AMPARs are expressed after eye-opening

After eye-opening, different time points were examined for Co^{2+} staining (i.e. P14, 18, 21, 26, 28, 33, 39 as well as 3 and 6 months). Based on the labelling pattern, we identified three distinct stages: P14–18, P21–28 and P33–6 months. In each case, Co^{2+} strongly labelled the cell bodies and dendrites of horizontal cells, demonstrating that the expression of Ca^{2+}-permeable AMPARs continued into adulthood (Fig. 4, left panels). Likewise, cell bodies of AII amacrine cells were stained by Co^{2+} throughout development; however, their dendrites were visible only in the first few days after eye-opening (e.g. P14–18). At later stages, processes arising from individual AII cells were indistinguishable from the appreciable staining of the entire IPL (e.g. P21–28). The IPL is a meshwork of bipolar cell axons and dendrites from amacrine and ganglion cells that each terminate into functionally distinct sublayers called sublamina a or b (Mumm *et al.* 2005) (Fig. 4, P21–28). The narrow dendritic arbor of AII amacrine cells, for example, traverses the entire IPL as revealed by filling individual cells with biocytin (Fig. 5*A*, left). It is interesting therefore that at all developmental stages examined, we did not observe a uniform intensity of staining in the IPL but that stronger labelling occurred in sublamina b (see arrow in Fig. 4, left, and also Fig. 5*B*, left). Indeed, statistical evaluation ($P < 0.05$, Student's two tailed, paired t test) of Co^{2+} labelling in the adult IPL revealed that the optical density of sublamina b (0.40 ± 0.03 arbitrary units (a.u.)) was almost 2-fold greater than sublamina a (0.25 ± 0.02 a.u.) (Fig. 5*B*, right).

It is unlikely that staining of the IPL arises solely from AII cell dendrites but that processes of other cell types also contribute. In support of this, the cell bodies of another population(s) of putative amacrine cells in the INL were clearly labelled during the first week following eye-opening and remained until P21–28. We did not attempt to determine their identity though, based on the position of the cell body (Menger & Wassle, 2000), the staining is consistent with A17 cells which are known to express Ca^{2+}-permeable AMPARs (Chavez *et al.* 2006). Similarly, we observed labelling of a population of cells in the GCL (e.g. P14 –P18) that disappeared during retinal maturation. As before, we did not examine this population

in detail though our observations are consistent with a previous study of Ca^{2+}-permeable AMPARs expressed by displaced amacrine cells and/or ganglion cells (Zhang *et al.* 1995).

To determine if Ca^{2+}-permeable AMPARs are blocked by extracellular polyamines after eye-opening, staining by 10 mM L-Glu was compared in the presence and absence of 50 μM PhTX (Fig. 4, right panels). At all postnatal stages tested, PhTX failed to completely block Co^{2+} staining of the cell bodies and dendrites of horizontal cells. In support of this, a comparison between the optical density of staining in the OPL in control (0.40 ± 0.02 a.u.) and PhTX-treated adult retinae (0.43 ± 0.05 a.u.) was statistically indistinguishable (Fig. 5*B*, right). For AII amacrine cells, the effect of PhTX was more complex. At stages P14–18 and P21–28, a subpopulation of AII cells was transiently PhTX insensitive. However, from postnatal period P33 onwards, staining of cell bodies was completely eliminated by PhTX (Fig. 4, lower right). In contrast, however, PhTX failed to completely block Co^{2+} staining in the IPL. In sublamina a, the intensity of staining was unchanged between control (0.25 ± 0.01 a.u.) and PhTX-treated (0.28 ± 0.03 a.u.) retina (Figs 4 and 5*B*, right). Interestingly, staining in sublamina b was reduced by almost 50% between control (0.40 ± 0.03 a.u.) and PhTX-treated (0.25 ± 0.03 a.u.) retinae (Fig. 5*B*, right). AII amacrine cells are innervated by two distinct presynaptic cell types each of which terminate in different sublamina of the IPL. Rod bipolar cells form ribbon synapses on the arboreal dendrites of sublamina b whereas OFF-cone bipolar cells form ribbon synapses on the arboreal dendrites of sublamina a (Kolb & Famiglietti, 1974; Strettoi *et al.* 1992; Chun *et al.* 1993; Veruki *et al.* 2003). As discussed below, the reduction of Co^{2+} staining in sublamina b and not sublamina a argues against the expression of a single population of Ca^{2+}-permeable AMPARs on AII cell dendrites, but rather, supports the segregation of pharmacologically distinct receptors into different sublaminae of the IPL (Fig. 5*A*, right).

Ca^{2+}-permeable AMPARs are resistant to block by other channel blockers

To examine if PhTX-insensitive AMPARs were resistant to other channel blockers, we compared Co^{2+} labelling elicited by 10 mM Glu in the presence and absence of Joro spider toxin (JSTX) (Blaschke *et al.* 1993) and IEM-1460 (Magazanik *et al.* 1997) (Fig. 6). Compared with the structure of PhTX, both JSTX and IEM-1460 differ in terms of their polyamine chain length and the chemical nature of the bulky headgroup (Fig. 6*A*). Consequently, if Co^{2+} staining due to Ca^{2+}-permeable AMPARs remained in the presence of all three blockers, our conclusions would not rely solely on the prescribed action of PhTX. In agreement with this, photomicrographs shown in Fig. 6*B* reveal that Co^{2+} staining elicited by L-Glu was principally unaffected by either JSTX (10 μM) or IEM-1460 (100 μM), similar to our findings with PhTX (50 μM). The IC_{50} value for block of recombinant AMPARs by IEM-1460 (at −80 mV) and JSTX (at −100 mV) is 1.6 μM (Magazanik *et al.* 1997) and 30 nM (Blaschke *et al.* 1993), respectively. In view of this, the blocker concentrations used in this experiment are supramaximal in nature, further strengthening our conclusion that the retina expresses Ca^{2+}-permeable AMPARs with novel pharmacological properties.

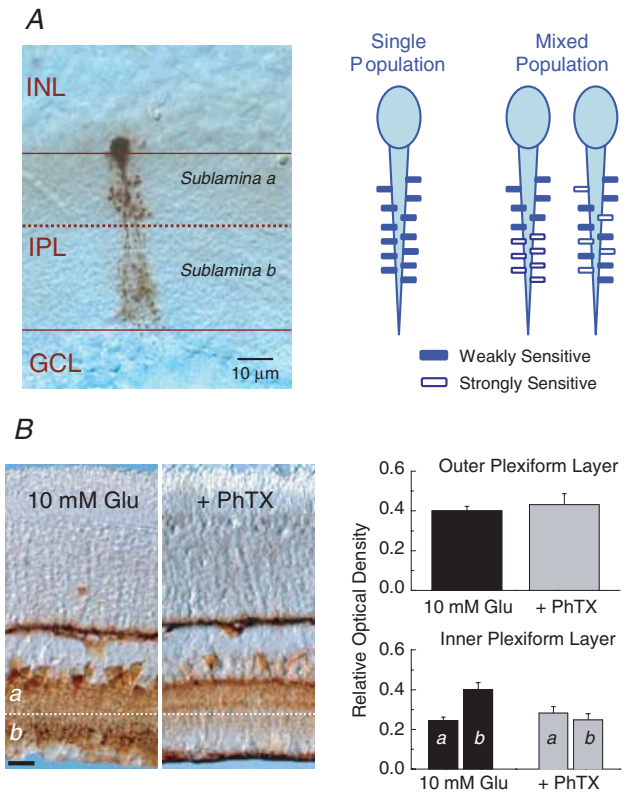

Figure 5. AII amacrine cell dendrites express two AMPAR populations
A, left, photomicrograph of an AII amacrine cell filled with biocytin reveals the extent of its dendritic arborization in the IPL. Right, schematic diagram showing the possible spatial arrangement of different AMPARs on dendrites of individual AII cells. *B*, left, photomicrographs comparing the effect of 50 μM PhTX (slide no. 260105-11R) on the staining elicited by 10 mM Glu (slide no. 260105-11R) in the IPL of a P36 retina. The dotted line demarcates between sublaminae a and b and the scale bar represents 20 μm. Right, images from bright-field microscope were obtained in black and white format and measurements of the relative optical density were determined for the OPL and sublaminae a and b of the IPL using an MCID Elite Image Analysis system (see Methods). A total number of eight images were obtained per treatment which was repeated for retinae taken from 8 adult rats. The data between different treatments were compared using a paired *t* test and expressed as the mean ± S.E.M.

AII amacrine cell synapses express PhTX-insensitive Ca^{2+}-permeable AMPARs

To test if PhTX-insensitive AMPARs are expressed at synapses, electrophysiological recordings of AII amacrine cells were performed on acutely isolated retinal slices. Figure 7*A* and *B* shows typical miniature EPSCs ($V_h = -70$ mV) recorded from the same AII cell in the absence and presence of 50 μM PhTX. In each case, synaptic activity was mediated by AMPARs since, as shown previously, all events were abolished by CNQX or GYKI 52466 (Fig. 2). In control conditions, mEPSC amplitude was best fitted by the sum of three Gaussian functions (Fig. 7*A*, red line) with amplitudes of -26.7 ± 1.6 pA, -18.4 ± 0.6 pA and -13.0 ± 0.1 pA ($n = 7$). Following bath perfusion of 50 μM PhTX, mEPSCs were not fully blocked, contrary to other studies (Toth & McBain, 1998) but instead were reduced in amplitude (Fig. 7*B*). In this case, amplitude distributions were best fitted by the sum of two Gaussian functions (Fig. 7*B*, red line) with values of -14.1 ± 0.1 pA and -12.0 ± 0.1 pA (Fig. 7*B*). Similar findings were observed in the absence of TTX suggesting that PhTX mainly acts postsynaptically and has little effect on neurotransmitter release. Finally, in agreement with our Co^{2+} staining experiments, spontaneous ($n = 4$) and miniature ($n = 7$) EPSCs resistant to PhTX block were observed in all AII amacrine cells tested irrespective of postnatal age (P19–P41, Fig. 7*C*).

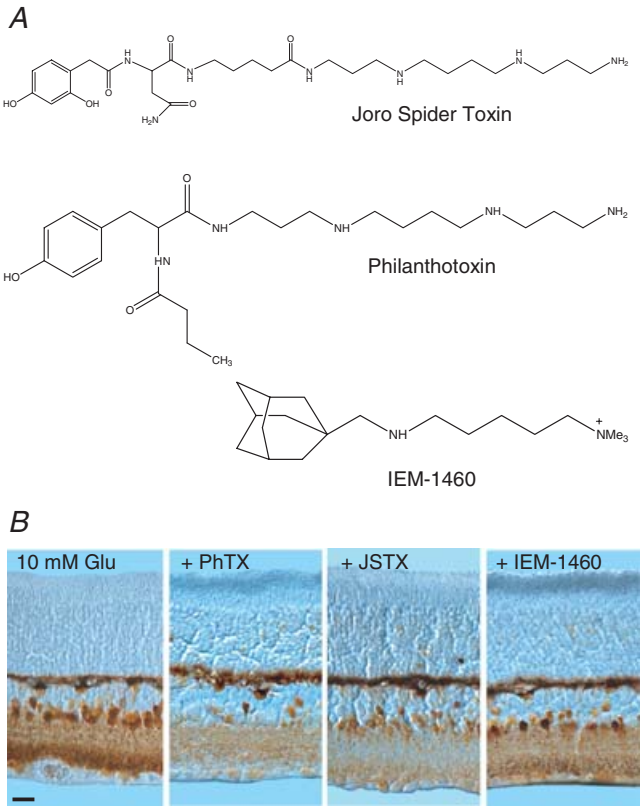

Figure 6. Retinal Ca^{2+}-permeable AMPARs are insensitive to a number of channel blockers
A, extended structure of PhTX, JSTX and IEM-1460 reveals differences in their polyamine chain length as well as the chemical nature of their bulky headgroup. *B*, photomicrographs comparing the effect of 50 μM PhTX (slide no. 081206-8R), 10 μM JSTX (slide no. 081206-9R) and 100 μM IEM-1460 (slide no. 081206-7L) on the intensity of Co^{2+} labelling elicited by 10 mM Glu (slide no. 081206-9L) in the same P26 retina. Like PhTX, channel blockers JSTX and IEM-1460 also failed to block staining in the IPL as well as cell bodies of horizontal and AII amacrine cells.

PhTX slows decay kinetics of synaptic AMPARs

To examine if the kinetic properties of PhTX-insensitive AMPARs are distinct, we initially compared averaged waveforms of mEPSCs in the presence and absence of PhTX. Figure 8*A* shows averaged waveforms from a typical recording that reveals a slowing in mEPSC decay kinetics in the presence of PhTX. A more detailed analysis of the decay kinetics of all events prior to the application of PhTX were best fitted by the sum of three exponential functions with time constants of 0.90 ± 0.01 ms, 1.25 ± 0.19 ms and 1.85 ± 0.60 ms (Fig. 8*B*). The kinetics of synaptic events observed in the presence of PhTX were best fitted by the sum of two and not three exponentials (Fig. 8*C*). The time constants estimated from the fit were 1.26 ± 0.03 ms and 1.53 ± 0.07 ms (Fig. 8*C*), each of which corresponded to the slower time constants observed in the control (Fig. 8*B*). This observation suggests that PhTX may differentiate between two kinetically distinguishable AMPAR synapses. That is, larger synaptic events have faster decay kinetics and are sensitive to PhTX block. In contrast, smaller events have slower decay kinetics and are insensitive to PhTX block. We reasoned that if this was the case, both fast and slow decaying synaptic events should be observed in control conditions. Consequently, control synaptic events of small amplitude (< -20 pA) should have slow decay kinetics identical to events observed in PhTX. However, analysis of small amplitude events revealed that their kinetic properties were dissimilar from events observed in PhTX (Fig. 8*D*). The time constants estimated from the fit of the data were 0.97 ± 0.01 ms and 1.37 ± 0.10 ms, which closely matches the two main kinetic components observed for events of all amplitude (Fig. 8*B*). This observation shows that PhTX does not distinguish between kinetically distinct AMPAR populations. The mechanism by which PhTX slows channel kinetics is not clear but may involve channel-trapping of external polyamines that, in turn, affects burst length (Bähring & Mayer, 1998). In summary, these observations demonstrate that all postsynaptic AMPARs expressed by AII amacrine cells bind PhTX but differ in their sensitivity to block.

Light entering the eye triggers expression of novel Ca^{2+}-permeable AMPARs

To directly test if light entering the eye triggers expression of PhTX-insensitive AMPARs, we repeated Co^{2+} staining

(Fig. 9) and electrophysiology experiments (Fig. 10) in retinae taken from dark-reared animals (see Methods). With Co^{2+} labelling, the staining elicited by L-Glu alone was comparable to light-adapted retinae (Fig. 9, left). In contrast, however, PhTX completely abolished staining of the cell bodies of AII cells as well as staining in the IPL (Fig. 9, right). For horizontal cells, Co^{2+} staining, though weak, was significantly reduced in intensity indicating that light may not be the only factor regulating the expression of PhTX-insensitive AMPARs (Fig. 9, right).

In agreement with Co^{2+} staining experiments, AMPAR synaptic activity recorded from AII amacrine cells in dark-reared animals (Fig. 10*A* and *C*), was fully abolished by 50 μM PhTX (Fig. 10*B* and *D*). In the light-deprived retina, the amplitude of synaptic events exhibited similar properties to responses in the light-adapted retina (Fig. 7) suggesting that dark-rearing apparently does not affect the number of AMPARs at postsynaptic densities. In agreement with this, the peak amplitude distribution was best fitted by the sum of three Gaussian functions (Fig. 10*C*, red line) with amplitudes of -31.4 ± 1.9 pA,

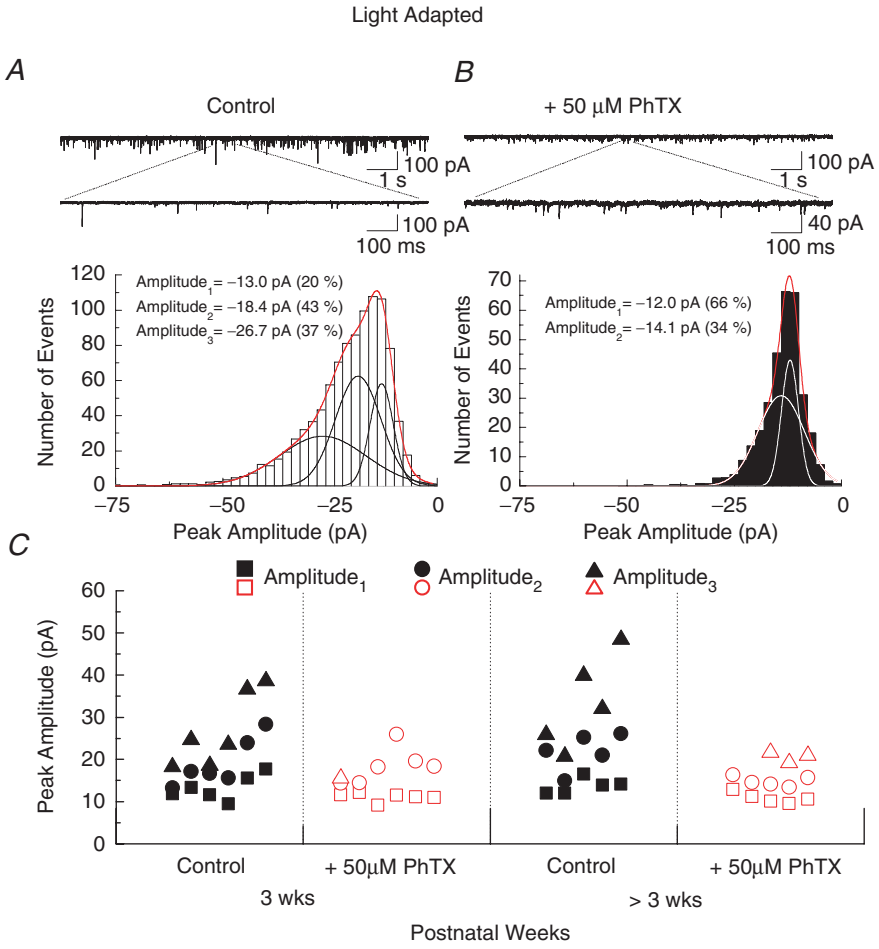

Figure 7. Synaptic AMPARs expressed by AII cells are resistant to PhTX block
A, upper, synaptic activity ($V_h = -70$ mV) recorded from an AII amacrine cell (cell no. 050131c2) in control conditions. Lower, summary plot from 7 cells showing that the amplitude of miniature synaptic events was fitted well by the sum of three Gaussian functions (red line). Individual Gaussian fits are shown as continuous black lines. Similar results were observed in the absence of TTX (data not shown). *B*, upper, in the same cell, bath application of 50 μM PhTX did not fully block synaptic activity but instead reduced peak response amplitude. Lower, in this case, the summary plot of peak synaptic current amplitude was fitted well by the sum of two Gaussian functions (red line). Individual Gaussian fits are shown as continuous white lines. *C*, plot summarizing the effect of PhTX on the amplitude of spontaneous ($n = 4$) and miniature ($n = 7$) synaptic events from 11 cells. In all cases, analysis was performed only in cells where synaptic events were recorded in presence and absence of 50 μM PhTX. Data have been grouped on whether recordings were performed on postnatal retina of 3 weeks ($n = 6$) or more ($n = 5$). Filled (control) and open (+ 50 μM PhTX) symbols (triangle, circle and square) in each column represent the value of the peak amplitude obtained from individual Gaussian fits. Note PhTX failed to fully block the synaptic activity in all AII amacrine cell recordings.

-19.9 ± 0.4 pA and -15.1 ± 0.1 pA ($n = 8$). Following bath perfusion of 50 μM PhTX, synaptic events were fully abolished (Fig. 10*B* and *D*), contrary to our observations in the light-adapted retina (Fig. 7). Taken together therefore the Co^{2+} staining and electrophysiology experiments from dark-reared animals demonstrate unequivocally that light entering the eye is critical for the expression of PhTX-insensitive Ca^{2+}-permeable AMPARs.

Discussion

Here we describe the expression of Ca^{2+}-permeable AMPARs with novel pharmacology in inhibitory retinal cells that lack synaptic NMDARs. At eye-opening, there is a developmental switch in receptor phenotype where Ca^{2+}-permeable AMPARs develop insensitivity to several well-known channel blockers: PhTX, IEM-1460 and JSTX. AMPARs exhibiting this novel pharmacology are absent from dark-reared animals demonstrating that light entering the eye is critical for their expression. Eye-opening and the expression of PhTX-insensitive AMPARs occurs at a time point when immature axons from bipolar cells are targeting specific sublamina of the IPL. The convergence of these events may identify the synapses of Ca^{2+}-permeable AMPARs as discriminatory targets for incoming axons of developing bipolar cells.

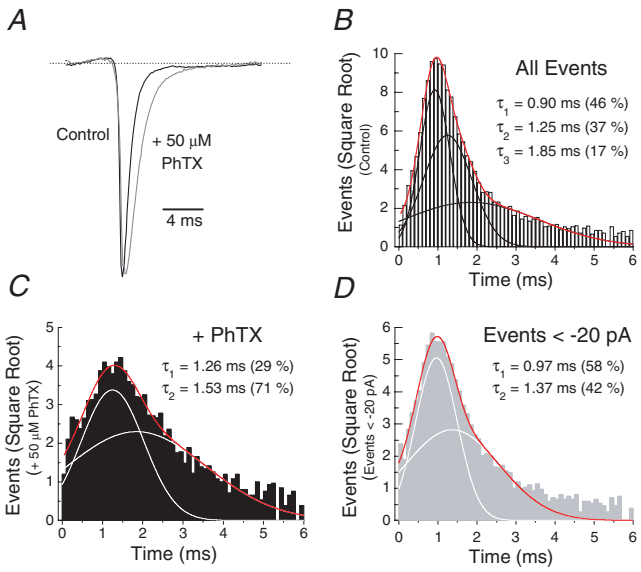

Figure 8. PhTX slows decay kinetics of synaptic AMPAR events
A, averaged mEPSCs from the same cell show differences in decay kinetics before and after application of PhTX (cell no. 050318c1). *B–D*, summary plots showing that the decay kinetics of synaptic events before (*B*) and after (*C*) PhTX application ($n = 7$) are different. *D*, the kinetic properties of events less than –20 pA are indistinguishable from the entire event population suggesting that PhTX slows decay kinetics of synaptic AMPARs.

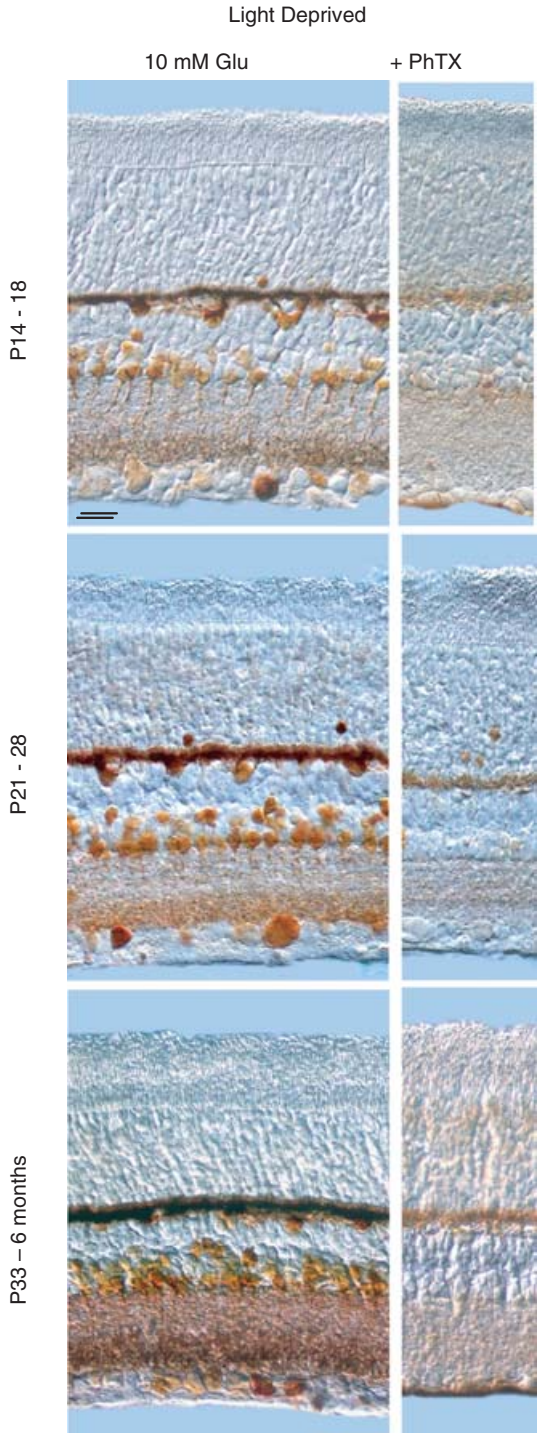

Figure 9. Inhibitory cells fail to express PhTX-insensitive Ca^{2+}-permeable AMPARs in dark-reared animals
Left panels, Co^{2+} staining pattern of horizontal and AII amacrine cells from dark-reared animals was similar to the light-adapted retina (P14–18, slide no. 010206-8R; P21–28, slide no. 050605-10L; P33–6 months, slide no. 210206-8L). Right panels, in contrast, however, 50 μM PhTX completely eliminated staining of AII cells and the IPL and significantly reduced Co^{2+} labelling of horizontal cells (P14–18, slide no. 010206-6L; P21–28, slide no. 050605-7L; P33–6 months, slide no. 210206-7R).

Developmental expression of Ca^{2+}-permeable AMPARs

Ca^{2+}-permeable AMPARs have been reported in either horizontal or AII amacrine cells of the retina of several vertebrates including rat (Morkve *et al.* 2002; Singer & Diamond, 2003; Veruki *et al.* 2003), salamander (Gilbertson *et al.* 1991), skate (Kreitzer *et al.* 2003) and cat (Pourcho *et al.* 2002); however, our study provides the first systematic description during postnatal development. Figure 11 summarizes our main finding that the vertebrate retina possesses distinct populations of Ca^{2+}-permeable AMPARs whose expression is regulated by light entering the eye (i.e. visual experience). Although we observed PhTX-insensitive AMPARs before eye-opening (i.e. P11, Figs 3 and 11, see arrows), experiments in dark-reared animals demonstrate that light entering through closed eyelids probably accounts for their expression. In horizontal cells, PhTX-sensitive AMPARs are present at birth until eye-opening. A developmental switch in their functional properties occurs, generating AMPARs with almost no sensitivity to polyamine block (Fig. 11*A*). Like horizontal cells, light entering the eye triggers expression of PhTX-insensitive AMPARs by AII amacrine cells (Fig. 11*B*). In this case, PhTX-insensitive receptors are transiently expressed on cell bodies but disappear as development proceeds (Fig. 11*B*). In the IPL, both PhTX-sensitive and -insensitive AMPARs are present following eye-opening (Fig. 11*B*, hatched bar). Interestingly, Co^{2+} staining experiments suggest that PhTX-sensitive AMPARs may be restricted to sublamina b (Figs 4 and 5*B*).

Comparison with other studies

We conclude that horizontal and AII cells express novel Ca^{2+}-permeable AMPARs based on their unexpected pharmacology. Specifically, we show insensitivity to three known channel blockers that are conventionally used in other studies at much lower concentrations. For example, Chavez *et al.* (2006) achieved full block of Ca^{2+}-permeable AMPARs in A17 retinal cells using as little as 1 μM PhTX, representing a concentration 50 times less than used in this study. Similarly, the IC_{50} value (−80 mV, $IC_{50} = 1.6\ \mu$M) for block of recombinant AMPARs (Magazanik *et al.* 1997) by IEM-1460 and block of native receptors by 500 nM JSTX (Bellone & Luscher, 2006) are also at concentrations 20–50 times lower than used in this study.

Numerous studies have routinely used PhTX as a pharmacological marker of Ca^{2+}-permeable AMPARs (Washburn & Dingledine, 1996; Washburn *et al.* 1997; Toth & McBain, 1998; Toth *et al.* 2000; Plant *et al.* 2006). In such instances, PhTX's use was based on the assumption that divalent permeability and cytoplasmic polyamine block have identical molecular determinants. In support of this, mutation of the Q/R site in the AMPAR pore affects both ion permeation and channel block (Bowie *et al.* 1999). However, mutation of another residue in the pore region affects only polyamine block (Dingledine *et al.* 1992), suggesting that it is possible to assemble AMPARs that

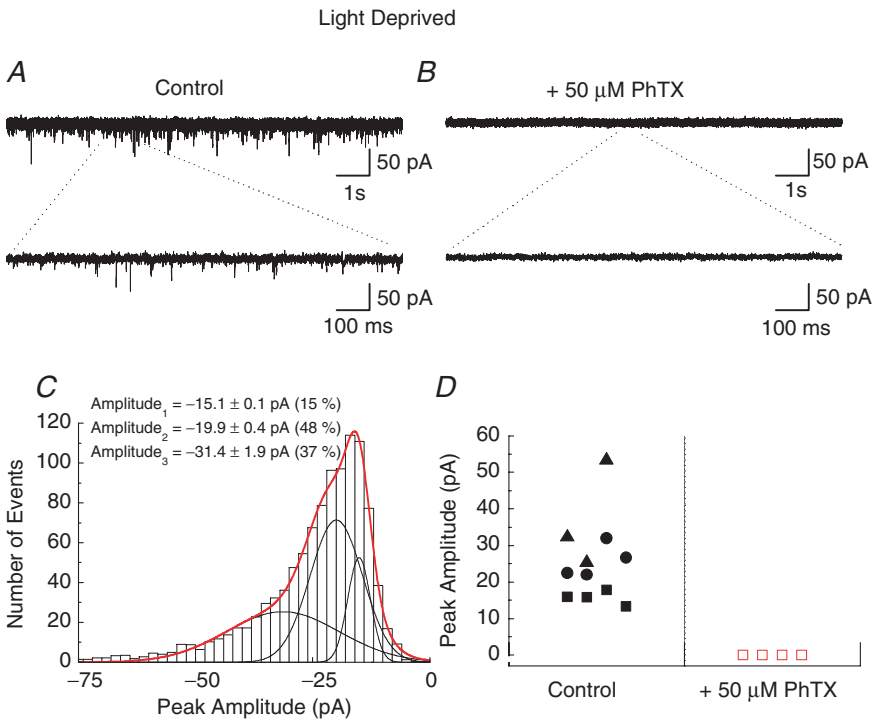

Figure 10. AMPAR synaptic activity in AII amacrine cells is abolished by PhTX in dark-reared animals
A, synaptic activity ($V_h = -70$ mV) recorded from an AII amacrine cell (cell no. 061117c2) in a retina taken from a dark-reared animal. *B*, in the same cell, bath application of 50 μM PhTX fully blocked synaptic activity in contrast to the light-adapted retina. *C*, summary plot from 8 cells showing that the peak amplitude of miniature synaptic events was fitted well by the sum of three Gaussian functions (red line). Individual Gaussian fits are shown as continuous black lines. *D*, plot summarizing the effect of PhTX on the amplitude of spontaneous AMPAR synaptic events recorded from dark-reared retina ($n = 4$). Filled (control) symbols (triangle, circle and square) in each column represent the value of the peak amplitude obtained from individual Gaussian fits.

exhibit Ca^{2+} permeability whilst lacking polyamine block. As discussed below, there are several possible molecular mechanisms that may account for this phenotype.

Does the retina express novel AMPARs?

The expression of Ca^{2+}-permeable AMPARs with novel pharmacology can be explained in several ways. One possibility is that PhTX insensitivity reflects the up-regulation of a scaffolding protein or phosphorylation event that changes the pharmacological properties of AMPARs. Although both mechanisms regulate AMPAR behaviour (Dingledine *et al.* 1999), accessory proteins or the phosphorylation state of the AMPAR have not been shown to affect pharmacology or ion permeation (see Mayer, 2005 for review). An alternative possibility is that the retina expresses a novel AMPAR subunit or that a known subunit undergoes alternate processing to affect PhTX sensitivity. There are several reasons to support either of these possibilities.

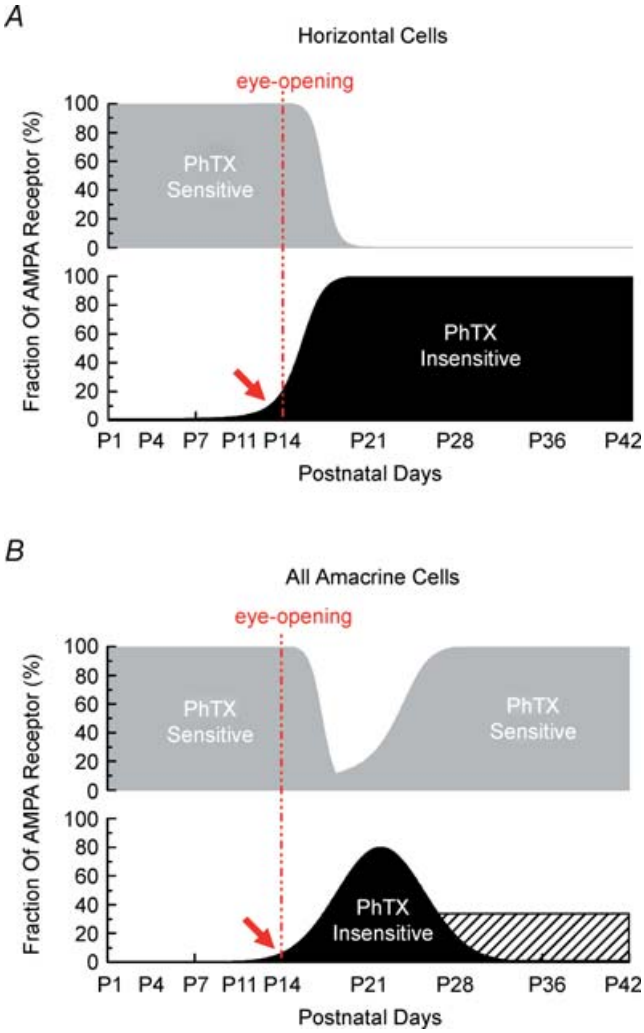

Figure 11. Expression of Ca^{2+}-permeable AMPARs is triggered by light entering the eye
Schematic diagrams intended to provide a qualitative description of the expression profile of Ca^{2+}-permeable AMPARs in AII and horizontal cells. The transient expression of Ca^{2+}-permeable AMPARs in other cells of the INL and GCL has not been included since it was not studied in detail. *A*, in horizontal cells, Ca^{2+}-permeable AMPARs sensitive to PhTX were replaced by AMPARs with little or no sensitivity to external polyamines after eye-opening. *B*, for AII amacrine cells, the expression profile is more complex. Prior to eye-opening, the cell bodies and dendrites of AII cells express PhTX-sensitive AMPARs. Like horizontal cells, AMPARs that are insensitive to PhTX are detected just before eye-opening (see arrows) and continue to be expressed on cell bodies and dendrites of AII cells in the first 3–4 weeks postnatal. However as development proceeds, the expression of PhTX-insensitive AMPARs is restricted to the IPL (hatched bar).

First, cloning studies during the 1990s focused their attention on cDNA libraries from CNS tissue that, for practical reasons, excluded the retina and spinal cord (Hollmann, 1999). To our knowledge, only one study has cloned AMPARs from the retina (Ueda, 1997). In this case, the author used a goldfish cDNA library and reported considerable diversity in mRNA phenotypes consistent with significant processing of primary transcripts. Second, cloning studies of other proteins involved in glutamate signalling, such as glutamate transporters (Eliasof *et al.* 1998) or metabotropic receptors (Nakajima *et al.* 1993), exhibit properties unique to the retina. Indeed, the retina is recognized as a CNS structure that often expresses novel signalling proteins, such as $GABA_C$ receptors (Feigenspan *et al.* 1993) that are expressed at much lower levels elsewhere in the CNS. Third and finally, several electrophysiological studies have identified non-NMDARs in the retina with atypical pharmacological properties (Ishida & Neyton, 1985; Aizenman *et al.* 1989; Gilbertson *et al.* 1991; Connaughton & Nelson, 2000). For example, Ishida & Neyton (1985) reported an unusual non-competitive antagonism of retinal AMPARs by receptor agonists that is not found in native (Patneau & Mayer, 1991) (e.g. hippocampus) and recombinant (Dingledine *et al.* 1999) AMPARs.

In summary, although the molecular basis by which AMPARs develop PhTX insensitivity remains to be established, our study highlights the identity of an AMPAR with novel pharmacological properties.

Physiological role of Ca^{2+}-permeable AMPARs

The physiological basis for the phenotypic switch and segregation of Ca^{2+}-permeable AMPARs is not clear. Elsewhere in the CNS, such as the brain stem (Rubio & Wenthold, 1997), hippocampus (Toth & McBain, 1998) and cerebellum (Landsend *et al.* 1997), iGluRs are targeted to specific postsynaptic sites in the same neuron suggesting that discrete expression of Ca^{2+}-permeable AMPARs may be an important facet of the role they fulfil in neurotransmission. In the retina, two mechanisms may be considered to account for our observations.

Firstly, light entering the eye may trigger expression of AMPARs with higher Ca^{2+} permeability to facilitate

synapse maturation. In the cerebellum, divalent permeability of AMPARs is dynamically regulated (Liu & Cull-Candy, 2000), which, based on our understanding of retinal ganglion cells (Wong & Wong, 2000), would help drive Ca^{2+}-dependent events that are undoubtedly required for inhibitory cell synapse maturation. An important caveat, however, is that unlike AMPARs in the cerebellum, both inhibitory cells we have studied express Ca^{2+}-permeable AMPARs throughout retinal development. Moreover, qualitative assessment of Co^{2+} staining intensity suggests that divalent permeability of inhibitory cell types is unchanged during development (cf. Fig. 3 and 4). Consequently, if a switch in divalent permeability occurs, it is likely to be modest in nature.

An alternative possibility is that the phenotypic change in AMPARs serves not to alter Ca^{2+} permeability but facilitate the establishment of lamina-specific connections. In support of this, we have shown that dendrites of AII cells express PhTX-sensitive AMPARs that are apparently segregated to sublamina b of the IPL (Figs 4 and 5*B*). On the presynaptic side, AII amacrine cells are innervated by ON bipolar cells that form synapses with their arboreal dendrites located in sublamina b of the adult (Kolb & Famiglietti, 1974; Veruki *et al.* 2003). However, during development, axons of ON bipolar cells extend and retract processes into both sublaminae a and b before the mature axonal arbor is finally established (Morgan *et al.* 2006). Interestingly, this process is not complete until P19–21 (Morgan *et al.* 2006) suggesting that PhTX-sensitive AMPARs are restricted to sublamina b in advance of axonal maturation. As yet, the molecular identity of lamination cues are not known; however, they are thought to be provided by amacrine cells and in place before bipolar cell stratification occurs (Morgan *et al.* 2006). In view of this, it would be interesting to test in future studies if distinct AMPARs, perhaps in concert with adhesion molecules (Yamagata *et al.* 2002), act as molecular guideposts to ensure faithful subcellular wiring of the IPL.

References

Aizenman E, Karschin A & Lipton SA (1989). Two pharmacological classes of quisqualate-induced electrical responses in rat retinal ganglion cells in vitro. *Eur J Pharmacol* **174**, 9–22.

Bähring R & Mayer ML (1998). An analysis of philanthotoxin block for recombinant rat GluR6(Q) glutamate receptor channels. *J Physiol* **509**, 635–650.

Bellone C & Luscher C (2006). Cocaine triggered AMPA receptor redistribution is reversed in vivo by mGluR-dependent long-term depression. *Nat Neurosci* **9**, 636–641.

Blaschke M, Keller BU, Rivosecchi R, Hollmann M, Heinemann S & Konnerth A (1993). A single amino acid determines the subunit-specific spider toxin block of alpha-amino-3-hydroxy-5-methylisoxazole-4-propionate/kainate receptor channels. *Proc Natl Acad Sci U S A* **90**, 6528–6532.

Bowie D, Bähring R & Mayer ML (1999). Block of kainate and AMPA receptors by polyamines and arthropod toxins. In *Handbook of Experimental Pharmacology; Ionotropic Glutamate Receptors in the CNS*, ed.Jonas P & Monyer H, pp. 251–373. Springer-Verlag, Berlin.

Bowie D, Lange GD & Mayer ML (1998). Activity-dependent modulation of glutamate receptors by polyamines. *J Neurosci* **18**, 8175–8185.

Burnashev N (1996). Calcium permeability of glutamate-gated channels in the central nervous system. *Curr Opin Neurobiol* **6**, 311–317.

Chavez AE, Singer JH & Diamond JS (2006). Fast neurotransmitter release triggered by Ca influx through AMPA-type glutamate receptors. *Nature* **443**, 705–708.

Chun MH, Han SH, Chung JW & Wassle H (1993). Electron-microscopic analysis of the rod pathway of the rat retina. *J Comp Neurol* **332**, 421–432.

Clements JD & Bekkers JM (1997). Detection of spontaneous synaptic events with an optimally scaled template. *Biophys J* **73**, 220–229.

Connaughton VP & Nelson R (2000). Axonal stratification patterns and glutamate-gated conductance mechanisms in zebrafish retinal bipolar cells. *J Physiol* **524**, 135–146.

Cull-Candy S, Kelly L & Farrant M (2006). Regulation of Ca^{2+}-permeable AMPA receptors: synaptic plasticity and beyond. *Curr Opin Neurobiol* **16**, 288–297.

Dingledine R, Borges K, Bowie D & Traynelis SF (1999). The glutamate receptor ion channels. *Pharmacol Rev* **51**, 7–61.

Dingledine R, Hume RI & Heinemann SF (1992). Structural determinants of barium permeation and rectification in non-NMDA glutamate receptor channels. *J Neurosci* **12**, 4080–4087.

Eliasof S, Arriza JL, Leighton BH, Kavanaugh MP & Amara SG (1998). Excitatory amino acid transporters of the salamander retina: identification, localization, and function. *J Neurosci* **18**, 698–712.

Famiglietti EV Jr & Kolb H (1975). A bistratified amacrine cell and synaptic cirucitry in the inner plexiform layer of the retina. *Brain Res* **84**, 293–300.

Feigenspan A, Wassle H & Bormann J (1993). Pharmacology of GABA receptor Cl^- channels in rat retinal bipolar cells. *Nature* **361**, 159–162.

Ge WP, Yang XJ, Zhang Z, Wang HK, Shen W, Deng QD & Duan S (2006). Long-term potentiation of neuron-glia synapses mediated by Ca^{2+}-permeable AMPA receptors. *Science* **312**, 1533–1537.

Gilbertson TA, Scobey R & Wilson M (1991). Permeation of calcium ions through non-NMDA glutamate channels in retinal bipolar cells. *Science* **251**, 1613–1615.

Greger IH, Khatri L, Kong X & Ziff EB (2003). AMPA receptor tetramerization is mediated by Q/R editing. *Neuron* **40**, 763–774.

Hartveit E & Veruki ML (1997). AII amacrine cells express functional NMDA receptors. *Neuroreport* **8**, 1219–1223.

Hollmann M (1999). Structure of ionotropic glutamate receptors. In *Handbook of Experimental Pharmacology: Ionotropic Glutamate Receptors in the CNS*, ed.Jonas P & Monyer H, pp. 1–98. Springer-Verlag, Berlin.

Ishida AT & Neyton J (1985). Quisqualate and L-glutamate inhibit retinal horizontal-cell responses to kainate. *Proc Natl Acad Sci U S A* **82**, 1837–1841.

Ishiuchi S, Tsuzuki K, Yoshida Y, Yamada N, Hagimura N, Okado H, Miwa A, Kurihara H, Nakazato Y, Tamura M, Sasaki T & Ozawa S (2002). Blockage of Ca^{2+}-permeable AMPA receptors suppresses migration and induces apoptosis in human glioblastoma cells. *Nat Med* **8**, 971–978.

Kalloniatis M, Sun D, Foster L, Haverkamp S & Wassle H (2004). Localization of NMDA receptor subunits and mapping NMDA drive within the mammalian retina. *Vis Neurosci* **21**, 587–597.

Kolb H & Famiglietti EV (1974). Rod and cone pathways in inner plexiform layer of cat retina. *Science* **186**, 47–49.

Kreitzer MA, Andersen KA & Malchow RP (2003). Glutamate modulation of GABA transport in retinal horizontal cells of the skate. *J Physiol* **546**, 717–731.

Krestel HE, Shimshek DR, Jensen V, Nevian T, Kim J, Geng Y, Bast T, Depaulis A, Schonig K, Schwenk F, Bujard H, Hvalby O, Sprengel R & Seeburg PH (2004). A genetic switch for epilepsy in adult mice. *J Neurosci* **24**, 10568–10578.

Laezza F, Doherty JJ & Dingledine R (1999). Long-term depression in hippocampal interneurons: joint requirement for pre- and postsynaptic events. *Science* **285**, 1411–1414.

Landsend AS, AmiryMoghaddam M, Matsubara A, Bergersen L, Usami S, Wenthold RJ & Ottersen OP (1997). Differential localization of delta glutamate receptors in the rat cerebellum: Coexpression with AMPA receptors in parallel fiber-spine synapses and absence from climbing fiber-spine synapses. *J Neurosci* **17**, 834–842.

Liu S-QJ & Cull-Candy SG (2000). Synaptic activity at calcium-permeable AMPA receptors induces a switch in receptor subtype. *Nature* **405**, 454–458.

Liu S, Lau L, Wei J, Zhu D, Zou S, Sun HS, Fu Y, Liu F & Lu Y (2004). Expression of Ca^{2+}-permeable AMPA receptor channels primes cell death in transient forebrain ischemia. *Neuron* **43**, 43–55.

Lukasiewicz PD, Eggers ED, Sagdullaev BT & McCall MA (2004). GABAC receptor-mediated inhibition in the retina. *Vision Res* **44**, 3289–3296.

Magazanik LG, Buldakova SL, Samoilova MV, Gmiro VE, Mellor IR & Usherwood PNR (1997). Block of open channels of recombinant AMPA receptors and native AMPA/kainate receptors by adamantane derivatives. *J Physiol* **505**, 655–663.

Mayer ML (2005). Glutamate receptor ion channels. *Curr Opin Neurobiol* **15**, 282–288.

Menger N & Wassle H (2000). Morphological and physiological properties of the A17 amacrine cell of the rat retina. *Vis Neurosci* **17**, 769–780.

Morgan JL, Dhingra A, Vardi N & Wong RO (2006). Axons and dendrites originate from neuroepithelial-like processes of retinal bipolar cells. *Nat Neurosci* **9**, 85–92.

Morkve SH, Veruki ML & Hartveit E (2002). Functional characteristics of non-NMDA-type ionotropic glutamate receptor channels in AII amacrine cells in rat retina. *J Physiol* **542**, 147–165.

Mumm JS, Godinho L, Morgan JL, Oakley DM, Schroeter EH & Wong RO (2005). Laminar circuit formation in the vertebrate retina. *Prog Brain Res* **147**, 155–169.

Nakajima Y, Iwakabe H, Akazawa C, Nawa H, Shigemoto R, Mizuno N & Nakanishi S (1993). Molecular characterization of a novel retinal metabotropic glutamate receptor mGluR6 with a high agonist selectivity for L-2-amino-4-phosphonobutyrate. *J Biol Chem* **268**, 11868–11873.

Oguni M, Setogawa T, Shinohara H & Kato K (1998). Calbindin-D 28 kD and parvalbumin in the horizontal cells of rat retina during development. *Curr Eye Res* **17**, 617–622.

Patneau DK & Mayer ML (1991). Kinetic analysis of interactions between kainate and AMPA: evidence for activation of a single receptor in mouse hippocampal neurons. *Neuron* **6**, 785–798.

Plant K, Pelkey KA, Bortolotto ZA, Morita D, Terashima A, McBain CJ, Collingridge GL & Isaac JT (2006). Transient incorporation of native GluR2-lacking AMPA receptors during hippocampal long-term potentiation. *Nat Neurosci* **9**, 602–604.

Pourcho RG, Qin P, Goebel DJ & Fyk-Kolodziej B (2002). Agonist-stimulated cobalt uptake provides selective visualization of neurons expressing. *J Comp Neurol* **454**, 341–349.

Pruss RM, Akeson RL, Racke MM & Wilburn JL (1991). Agonist-activated cobalt uptake identifies divalent cation-permeable kainate receptors on neurons and glial cells. *Neuron* **7**, 509–518.

Rapaport DH, Wong LL, Wood ED, Yasumura D & LaVail MM (2004). Timing and topography of cell genesis in the rat retina. *J Comp Neurol* **474**, 304–324.

Rozov A & Burnashev N (1999). Polyamine-dependent facilitation of postsynaptic AMPA receptors counteracts paired-pulse depression. *Nature* **401**, 594–598.

Rubio ME & Wenthold RJ (1997). Glutamate receptors are selectively targeted to postsynaptic sites in neurons. *Neuron* **18**, 939–950.

Singer JH & Diamond JS (2003). Sustained Ca^{2+} entry elicits transient postsynaptic currents at a retinal ribbon synapse. *J Neurosci* **23**, 10923–10933.

Strettoi E, Raviola E & Dacheux RF (1992). Synaptic connections of the narrow-field, bistratified rod amacrine cell (Aii) in the rabbit retina. *J Comp Neurol* **325**, 152–168.

Thiagarajan TC, Lindskog M & Tsien RW (2005). Adaptation to synaptic inactivity in hippocampal neurons. *Neuron* **47**, 725–737.

Toth K & McBain CJ (1998). Afferent-specific innervation of two distinct AMPA receptor subtypes on single hippocampal interneurons. *Nat Neurosci* **1**, 572–578.

Toth K, Suares G, Lawrence JJ, Philips-Tansey E & McBain CJ (2000). Differential mechanisms of transmission at three types of mossy fiber synapse. *J Neurosci* **20**, 8279–8289.

Ueda H (1997). Multiple forms of AMPA-type glutamate receptor mRNA phenotypes in goldfish retina and tectum. *Gen Pharmacol* **29**, 575–581.

van Zundert B, Yoshii A & Constantine-Paton M (2004). Receptor compartmentalization and trafficking at glutamate synapses: a developmental proposal. *Trends Neurosci* **27**, 428–437.

Veruki ML, Morkve SH & Hartveit E (2003). Functional properties of spontaneous EPSCs and non-NMDA receptors in rod amacrine (AII) cells in the rat retina. *J Physiol* **549**, 759–774.

Washburn MS & Dingledine R (1996). Block of alpha-amino-3-hydroxy-5-methyl-4-isoxazolepropionic acid (AMPA) receptors by polyamines and polyamine toxins. *J Pharmacol Exp Ther* **278**, 669–678.

Washburn MS, Numberger M, Zhang S & Dingledine R (1997). Differential dependence on GluR2 expression of three characteristic features of AMPA receptors. *J Neurosci* **17**, 9393–9406.

Wong WT, Myhr KL, Miller ED & Wong RO (2000). Developmental changes in the neurotransmitter regulation of correlated spontaneous retinal activity. *J Neurosci* **20**, 351–360.

Wong WT & Wong RO (2000). Rapid dendritic movements during synapse formation and rearrangement. *Curr Opin Neurobiol* **10**, 118–124.

Yamagata M, Weiner JA & Sanes JR (2002). Sidekicks: synaptic adhesion molecules that promote lamina-specific connectivity in the retina. *Cell* **110**, 649–660.

Zhang D, Sucher NJ & Lipton SA (1995). Co-expression of AMPA/kainate receptor-operated channels with high and low Ca^{2+} permeability in single rat retinal ganglion cells. *Neuroscience* **67**, 177–188.

Acknowledgements

This work was supported by an operating grant from the N.I.H. (Grant MH62144) and graduate student fellowships from the FRSQ Vision Network and McGill Faculty of Medicine to I.K.O. D.B. is the recipient of a Canada Research Chair award in Receptor Pharmacology. We thank Drs P. Clarke and A. Ribeiro-Da-Silva for access to their cryostat and microscope facility, respectively, and Drs A. Di Polo, G. Maccaferri, R. A. McKinney, E. S. Ruthazer and members of the Bowie lab for interesting discussions and comments on the manuscript.